

Flue gas CO₂ mineralization using thermally activated serpentine: From single- to double-step carbonation

Electronic Supplementary Information

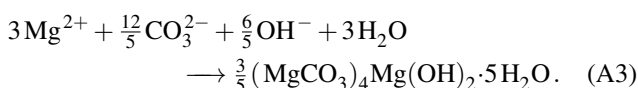
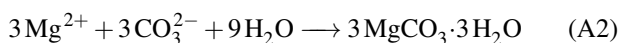
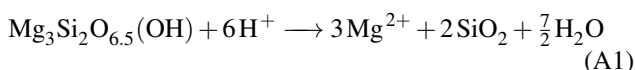
Content

Appendix A:	Extent of carbonation by TGA analysis	page 2
Appendix B:	Characterization of the solid product from single-step experiments	page 3
Appendix C:	Characterization of the solid product from double-step experiments	page 4
Fig. S1:	Experimental evidence for transformation in the MgO–CO ₂ –H ₂ O system	page 9
Fig. S2:	Complete pH profiles in the dissolution reactor during double-step experiments	page 10

A Extent of carbonation by TGA analysis

A.1 Derivation of Eq. (1)

Unlike for non-hydrated silicate minerals such as wollastonite (CaSiO_3) or forsterite (Mg_2SiO_4), the carbonation of partially dehydroxylated lizardite leads to a stoichiometric mismatch of the elements present in the starting material and the elements contained in the residue after TGA. This is evident from the corresponding dissolution and precipitation reactions of partially dehydroxylated lizardite with 25 mol % residual hydroxyls. Ignoring the impurities present in our PDL and its deviations from the ideal stoichiometry of lizardite, as well as presuming that the Mg-carbonate produced consists of either nesquehonite ($\text{MgCO}_3 \cdot 3\text{H}_2\text{O}$) or dypingite ($(\text{MgCO}_3)_4\text{Mg}(\text{OH})_2 \cdot 5\text{H}_2\text{O}$), the carbonation reactions are given by:



In this study, we have determined the mass fraction of CO_2 in a TGA sample, x_{CO_2} , based on the TGA sample mass at 350°C , $m_s^{\text{TGA}}|_{T=350^\circ\text{C}}$, corresponding to the temperature at which all physisorbed water, the crystal water, and the hydroxyls are already removed. After the decarbonation step during TGA, the solid residue consists of $\text{Mg}_3\text{Si}_2\text{O}_7$. Hence, compared to the mass of the unreacted PDL (prior to carbonation) associated to the TGA sample, $m_{s,0}^{\text{TGA}}$, the mass of the TGA residue after decarbonation, $m_s^{\text{TGA}}|_{T_{\text{res}}}$, is reduced by the mass $m_{\text{OH},0}^{\text{TGA}}$, which corresponds to the weight of the hydroxyl in the unreacted PDL that is lost as half a mole of H_2O per three moles of CO_2 mineralized in the form of nesquehonite, or per 12/5 moles of CO_2 mineralized in the form of dypingite. Further reductions of $m_{s,0}^{\text{TGA}}$ arise from the mass of the aqueous Mg and Si, $m_{\text{Mg},l}^{\text{TGA}}$ and $m_{\text{Si},l}^{\text{TGA}}$, that are present in the liquor associated to the part of a slurry sample of which the dried solids were subjected to TGA. Combining these quantities yields

$$1 - x_{\text{CO}_2} = \frac{m_s^{\text{TGA}}|_{T_{\text{res}}}}{m_s^{\text{TGA}}|_{T=350^\circ\text{C}}} = \frac{m_{s,0}^{\text{TGA}} - m_{\text{OH},0}^{\text{TGA}} - m_{\text{Mg},l}^{\text{TGA}} - m_{\text{Si},l}^{\text{TGA}}}{m_s^{\text{TGA}}|_{T=350^\circ\text{C}}}, \quad (\text{A4})$$

with

$$x_{\text{CO}_2} = \frac{m_s^{\text{TGA}}|_{T=350^\circ\text{C}} - m_s^{\text{TGA}}|_{T_{\text{res}}}}{m_s^{\text{TGA}}|_{T=350^\circ\text{C}}}. \quad (\text{A5})$$

The water loss term of the quotient on the right hand side of Eq. (A4) is proportional to x_{CO_2} , which reads

$$\frac{m_{\text{OH},0}^{\text{TGA}}}{m_s^{\text{TGA}}|_{T=350^\circ\text{C}}} = \gamma \frac{M_{\text{H}_2\text{O}}}{M_{\text{CO}_2}} x_{\text{CO}_2}, \quad (\text{A6})$$

where $M_{\text{H}_2\text{O}}$ and M_{CO_2} are the molar masses of water and CO_2 , respectively. Following from Eqs. (A1 – A3), the parameter γ is equal to $1/2\mu^{-1}$ for nesquehonite or to $5/8\mu^{-1}$ for dypingite, where μ is the stoichiometric index of Mg.

The mass of the aqueous Mg in Eq. (A4) was obtained from the known total mass of each slurry sample, $m_{\text{tot}}^{\text{sam}}$, the total dry weight of the solids therein, m_s^{sam} , the mass of the TGA sample at the starting temperature, $m_s^{\text{TGA}}|_{T_{\text{start}}}$, the concentration of Mg measured in the sample liquor, c_{Mg} , and its molar mass, M_{Mg} :

$$m_{\text{Mg},l}^{\text{TGA}} = \frac{m_s^{\text{TGA}}|_{T_{\text{start}}}}{m_s^{\text{sam}}} (m_{\text{tot}}^{\text{sam}} - m_s^{\text{TGA}}|_{T_{\text{start}}}) c_{\text{Mg}} M_{\text{Mg}}. \quad (\text{A7})$$

The same equation applies to $m_{\text{Si},l}^{\text{TGA}}$, replacing the concentration and molar mass with the corresponding values for Si, c_{Si} and M_{Si} .

With this information, Eq. (A4) can be rewritten as

$$m_s^{\text{TGA}}|_{T=350^\circ\text{C}} = \frac{m_{s,0}^{\text{TGA}}}{1 - x_{\text{CO}_2} + \gamma \frac{M_{\text{H}_2\text{O}}}{M_{\text{CO}_2}} x_{\text{CO}_2} + \frac{m_{\text{Mg},l}^{\text{TGA}} + m_{\text{Si},l}^{\text{TGA}}}{m_s^{\text{TGA}}|_{T=350^\circ\text{C}}}}. \quad (\text{A8})$$

The extent of carbonation, R_x , is derived from

$$R_x = \frac{n_{\text{Mg,nesq.}}^{\text{TGA}}}{n_{\text{Mg},0}^{\text{TGA}}} = \frac{0.8n_{\text{Mg,dyp.}}^{\text{TGA}}}{n_{\text{Mg},0}^{\text{TGA}}} = \frac{x_{\text{CO}_2} m_s^{\text{TGA}}|_{T=350^\circ\text{C}}}{m_{\text{Mg},0}^{\text{TGA}}} \frac{M_{\text{Mg}}}{M_{\text{CO}_2}}, \quad (\text{A9})$$

where $n_{\text{Mg,nesq.}}^{\text{TGA}}$ and $n_{\text{Mg,dyp.}}^{\text{TGA}}$ are the number of moles of Mg contained in the TGA sample in the form of the two carbonates (nesq. and dyp.), $n_{\text{Mg},0}^{\text{TGA}}$ and $m_{\text{Mg},0}^{\text{TGA}}$ are the amount of moles of Mg and the mass of Mg in the unreacted PDL associated to the TGA sample. Note that the latter mass divided by the mass $m_{s,0}^{\text{TGA}}$ represents the mass fraction of Mg of our PDL material, i.e. $x_{\text{Mg},0} = 23.95\%$. Upon inserting Eqs. (A8) into (A9) one finds the explicit expression for the mass correction parameter C in Eq. (1) of the main text, so as this writes:

$$R_x = \frac{x_{\text{CO}_2}}{1 - x_{\text{CO}_2} + \gamma \frac{M_{\text{H}_2\text{O}}}{M_{\text{CO}_2}} x_{\text{CO}_2} + \frac{m_{\text{Mg},l}^{\text{TGA}} + m_{\text{Si},l}^{\text{TGA}}}{m_s^{\text{TGA}}|_{T=350^\circ\text{C}}}} \frac{M_{\text{Mg}}}{x_{\text{Mg},0} M_{\text{CO}_2}}. \quad (\text{A10})$$

A.2 Comparison of TGA and TIC analysis

In literature, one finds a rather broad range for the decarbonation temperature of Mg-carbonates. In fact, particularly for

Mg-carbonates, TGA analysis is susceptible to variations in the heating rate, isothermal sections, sample amount, and gas atmosphere [Hollingbery *et al.*, *Thermochimi. Ac.*, 2010, **509**, 1–11]. In order to narrow down this temperature range, 16 samples from test experiments at all four temperatures and with $S/L = 10\%$ wt. were additionally analyzed for their total inorganic carbon content (TIC; VCPH-Analyzer, Shimadzu). To calculate the extent of carbonation, Eq. (A10) can be modified to yield

$$R_x = \frac{x_C}{1 - \frac{M_{\text{incr.}}}{M_C} x_C + \gamma \frac{M_{\text{H}_2\text{O}}}{M_C} x_C} \frac{M_{\text{Mg}}}{x_{\text{Mg},0} M_C}, \quad (\text{A11})$$

where x_C is the quantity obtained from the TIC analysis, i.e. the mass fraction of carbon, and M_C is the molar mass of carbon. Since in this case x_C is determined based on the weight of the total solid product, the correction for the weight increase due to carbonation in Eq. (A11) has to include also the crystal water and hydroxyls that are present in the Mg-carbonates. This mass increase is given by the weight of one mole of CO_2 plus 3 moles of H_2O per mole of carbon in the case of nesquehonite ($M_{\text{incr.}} = 98 \text{ g mol}^{-1}$), and by the weight of one mole of CO_2 plus 1.5 moles of H_2O in the case of dypingite ($M_{\text{incr.}} = 71 \text{ g mol}^{-1}$). Note that the Mg- and Si-concentration were not measured for these test experiments, hence the corresponding mass corrections were not included in the calculations of R_x using Eqs. (A10) and (A11).

By comparing the TIC-based R_x values with those obtained from TGA, it was found that the two analytical techniques were in excellent agreement ($R^2 = 0.98$) under the following three conditions: 1) when the background of unreacted material (averaged over five measurements) was subtracted from the TGA profiles of the carbonated samples; 2) when taking $T_{\text{res.}} = 500^\circ\text{C}$ to calculate x_{CO_2} using Eq. (A5) for samples containing nesquehonite; and 3) when taking $T_{\text{res.}} = 550^\circ\text{C}$ for samples containing the hydrated-basic Mg-carbonate. All R_x values reported in this study are based on TGA profiles interpreted in this way, applying also the mass correction for the aqueous solutes.

B Characterization of the solid product from single-step experiments

In Fig. B1, the XRD spectra of the final product for the four experiments with $S/L = 20\%$ wt. are shown together with the spectra of the unreacted PDL for comparison. For the experiment at 60°C , the spectra of all eight samples are included. The main peaks of nesquehonite are featured in the 30°C and 50°C spectra, as well as in the 60°C series up to the sixth sample after 240 min, but they are absent in the two remaining 60°C spectra and in the 90°C spectrum. Instead, the latter spectra show the two main peaks of dypin-

gite ($(\text{MgCO}_3)_4 \cdot \text{Mg}(\text{OH})_2 \cdot 5 \text{H}_2\text{O}$) and hydromagnesite (the same is true for the spectra of the earlier 90°C samples, not shown in Fig. B1). However, the first peak from the left, which could discriminate between these two basic-hydrated Mg-carbonates, falls right in between the corresponding low angle feature of the reference spectra, located at $2\theta \approx 8.3^\circ$ and 9.6° , respectively. This indicates that the Mg-carbonate in the final product of the 60°C and 90°C experiments consisted of either an intermediate species or a mineral in transformation rather than of a pure solid of well defined composition. In fact, we found that said peak shifts to the right, *i.e.* towards the reference peak of hydromagnesite, when the product collected after a high temperature experiment is put back into the filtered solution and kept at the same T and $p\text{CO}_2$ for an additional period of 8 h (see Fig. S1c†).

The spectra measured for samples containing nesquehonite feature a broad peak centered at around $2\theta \approx 16.6^\circ$. The only mineral of the Mg-carbonate family that exhibits a peak at this angle is artinite ($\text{MgCO}_3\text{Mg}(\text{OH})_2 \cdot 3 \text{H}_2\text{O}$), of which a reference spectrum is included in Fig. B1. We believe that this feature is an artifact originating from the drying of the sampled solids under vacuum at 40°C . Although previously washed, the filter cake may have still contained mother liquor in pores and cleats, which could provide the Mg required to transform nesquehonite into the basic-hydrated artinite. The liquor of the experiments at 30°C was the richest in Mg, which could explain why the 16.6° peak is strongest for the 30°C spectrum, where the main peaks of nesquehonite are correspondingly weaker. Since such transformation was likely limited by the availability of Mg from the remaining liquor, the unknown 16.6° peak might be specific of a metastable intermediate that does not exhibit the other artinite reference peaks yet. Note, however, that the lack of CO_2 under vacuum conditions prevented any further carbonation, so as this artifact would not affect the carbonation efficiency measured by TGA after drying.

Fig. B2 shows SEM images of the same final samples described above, together with EDX spot measurements of six locations in these images. The images confirm the needle-like and platelet-like morphology of nesquehonite/artinite and dypingite/hydromagnesite, respectively. As expected, the EDX spectra derived from spots focused on these crystals exhibit peaks for carbon (C), oxygen (O), and Mg. Rounded and irregular particles of partly reacted PDL can be easily distinguished, and the correspondingly positioned EDX spectra confirm the presence of Si and of little Fe in addition to O and Mg (spot 3 and 5 in Fig. B2b,c). Traces of Si in the carbonate spectra and traces of C in the PDL spectra could be associated to background effects from PDL fines and/or re-precipitated silica and from the graphite glue on the sample holder, respectively.

C Characterization of the solid product from double-step experiments

Exemplary for all double-step experiments, Fig. C1 shows the XRD spectra of the final solid products of experiment DS6 (stepwise T -ramp). The spectra of the unreacted PDL and of the seeds used in this campaign are included for comparison. The spectrum of the PDL residue shows no signs of carbonates, confirming that the formation of Mg-carbonates was effectively avoided in the first step and outsourced to the precipitator. The spectrum of the precipitate is identical to the one of the seeds, thus confirming that crystal growth could proceed without going through nucleation of a different carbonate species. Note that the spectra of the basic-hydrated carbonate exhibit a small peak at at $2\theta \approx 26.2^\circ$, which coincides with the main feature of both quartz and the Ca-carbonate aragonite. While the presence of small amounts of quartz is quite likely, also a Ca-carbonate could be present, since this element is contained as an impurity in the PDL. We have other evidence for the presence of traces of a Ca-carbonate from the Raman measurements, however, further elucidation of these product impurities is beyond the scope of this study.

For the same experiment shown in Fig. C1, two SEM images and an EDX measurement are presented in Fig. C2. The images show rosettes of platy crystals that are typical for dypingite and/or hydromagnesite (see references in Section 2.3.4 of main text).

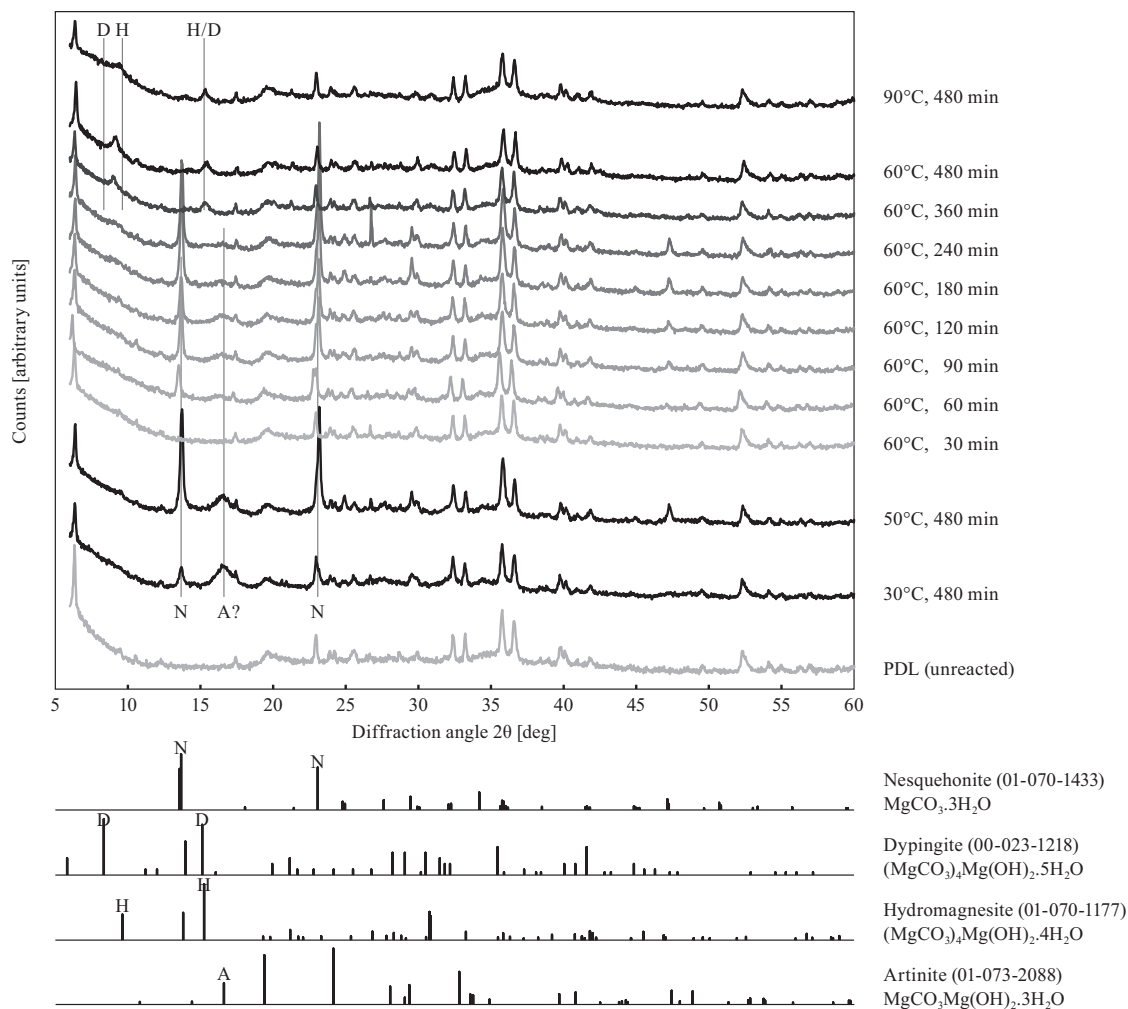


Fig. B1 XRD spectra of the solid product sampled during experiments with $S/L = 20\%$ wt.. Temperature and sampling time is indicated on the right. Also shown for comparison are the spectrum of unreacted PDL (see [Werner *et al.*, *Chem. Eng. J.*, 2014, **241**, 301–313] for peak identification) and reference patterns of the best matching phases (EVA software, Bruker). For better visual guidance, the position of the characteristic peaks discussed in the text are indicated by gray vertical lines.

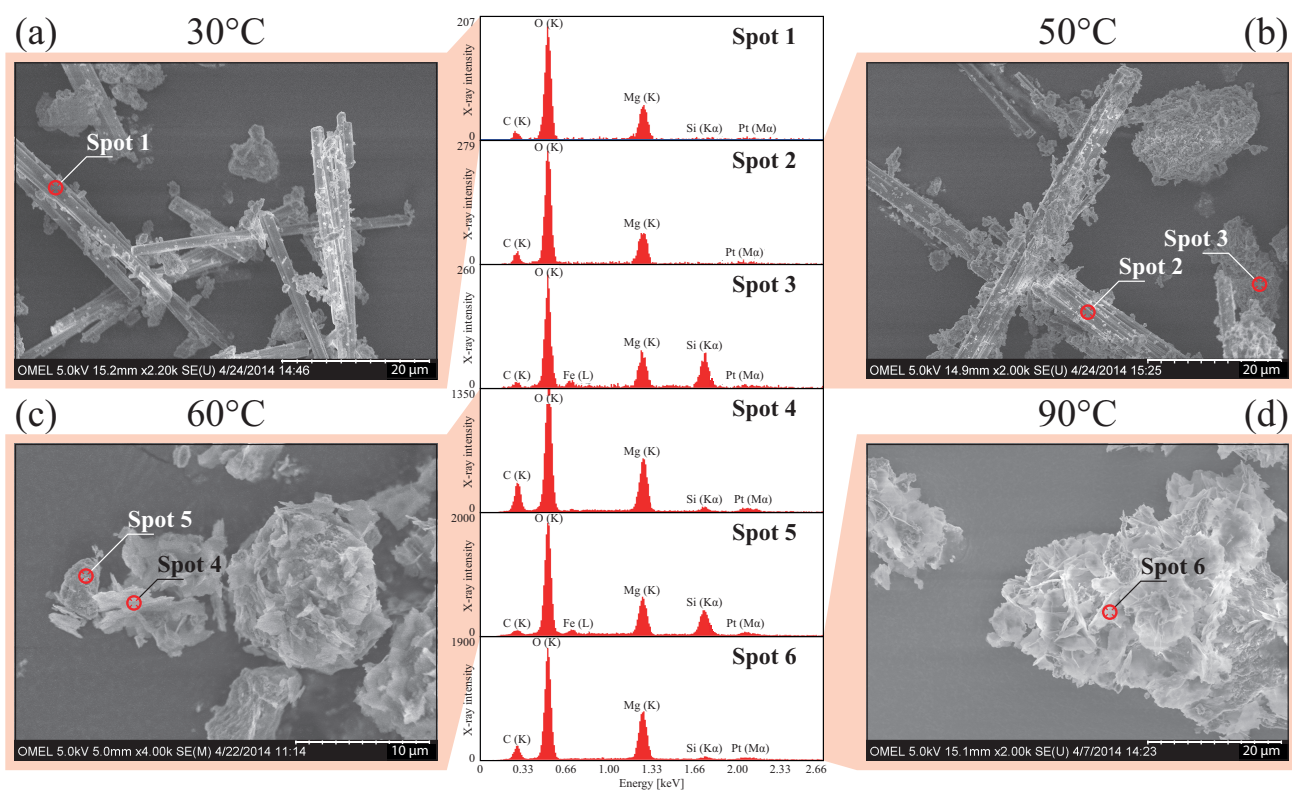


Fig. B2 SEM images and six EDX spot measurements of the final sample collected for experiments with $S/L = 20\%$ wt. at (a, Spot 1) 30 °C, (b, Spot 2,3) 50 °C, (c, Spot 4,5) 60 °C, and (d, Spot 6) 90 °C. The small platinum (Pt) peak originates from coating the samples with a thin layer of this element for enhanced SEM contrast.

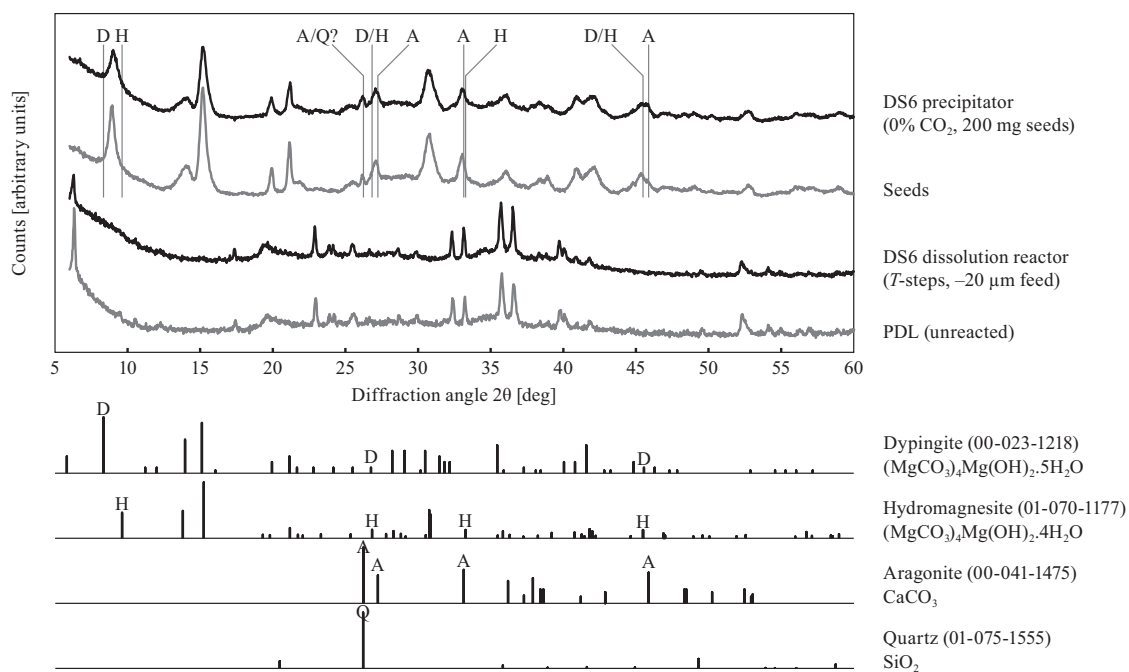


Fig. C1 XRD spectra of the final product collected from the double-step experiment DS6. Also shown for comparison are the spectra of the seeds that were used in all double-step experiments, of the unreacted PDL (see [Werner *et al.*, *Chem. Eng. J.*, 2014, **241**, 301–313] for peak identification), and the reference patterns of the best matching phases (EVA software, Bruker). For better visual guidance, the position of the characteristic peaks discussed in the text are indicated by gray vertical lines.

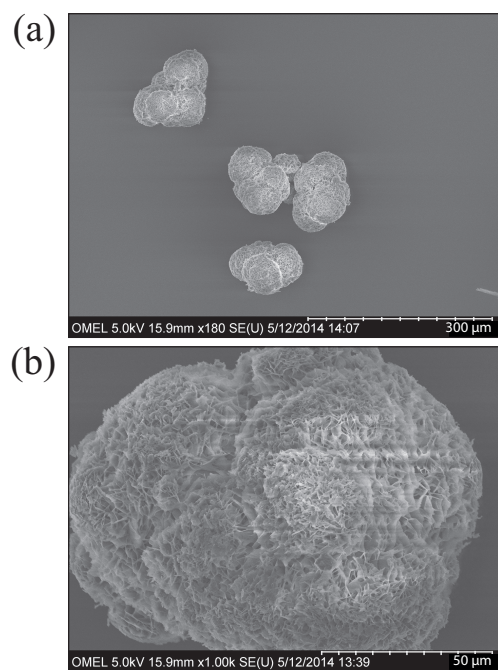


Fig. C2 (a,b) SEM images and (c) EDX spot measurement of the final product in the precipitator collected from the double-step experiment DS6. The small platinum (Pt) peak in (c) originates from coating the samples with a thin layer of this element for enhanced SEM contrast.

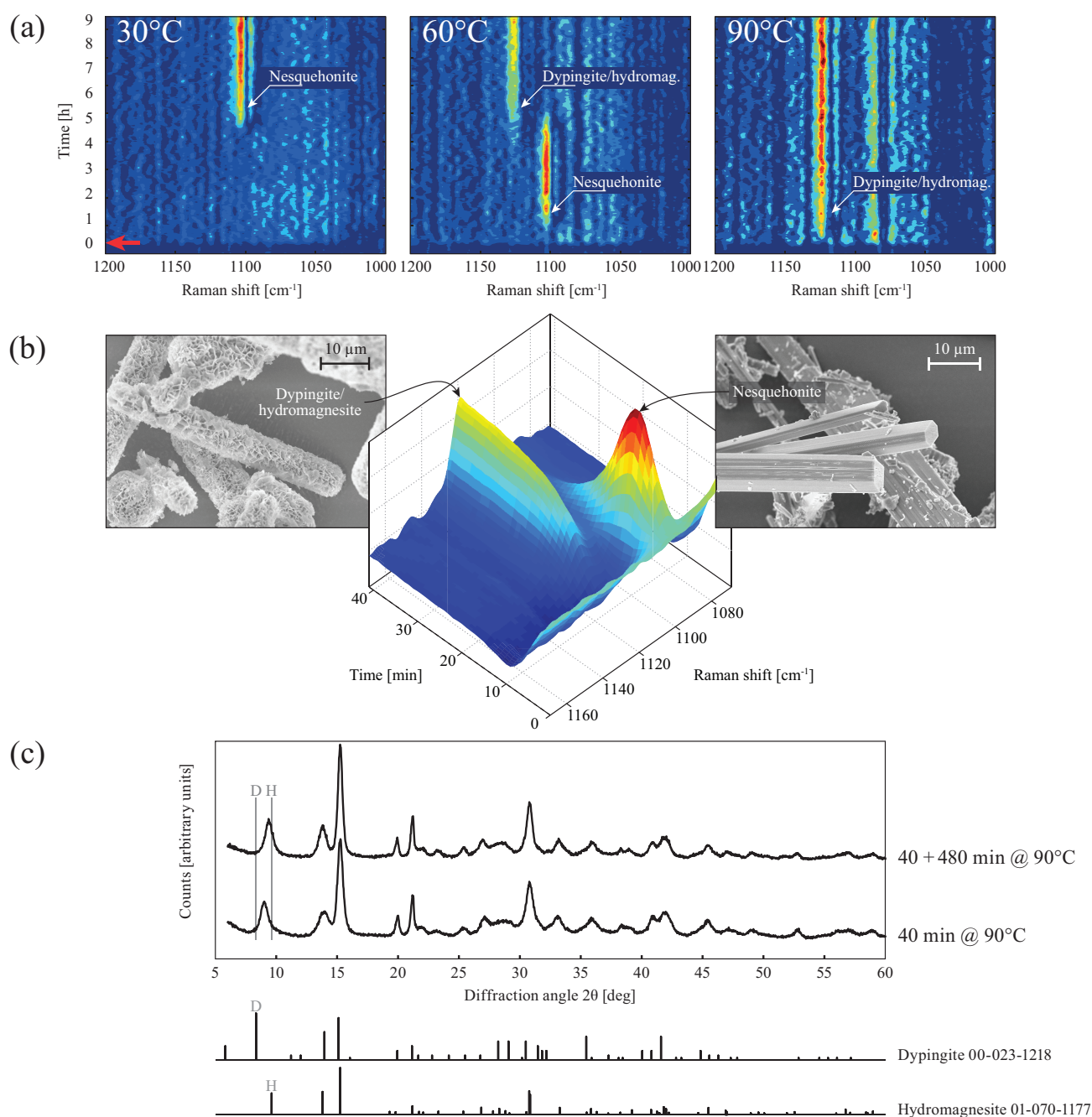


Fig. S1 Experimental evidence for transformation in the PDL–CO₂–H₂O system at moderate T and low $p\text{CO}_2$: (a) Contour plots of Raman spectra with color map relative to gradient of spectra in x-direction, measured during test experiments at 30, 60, and 90 °C, with a feed gas of pure CO₂, and $S/L = 10\%$ wt.. The red arrow indicates the time when the solid feed was added. The Raman shift wavenumber of nesquehonite and dypingite/hydromagnesite are 1099 cm⁻¹ and 1119 cm⁻¹, respectively. Transformation from the former into the latter takes place at 60 °C at ~ 5 h. (b) Raman spectra showing the same transformation taking place when quickly heating an Mg-rich liquor up to 90 °C in a reactor with 2.5 % CO₂ in the feed gas (the liquor stemming from the dissolution step of a T -swing test experiment at 30 °C and 100 % CO₂). The SEM images show the typical morphology of nesquehonite precipitating when keeping the same liquor at atmospheric conditions for several days, as well as the honeycomb texture of platy crystals typical for dypingite/hydromagnesite. Interestingly, the elongated habit of nesquehonite was largely preserved during transformation. (c) The XRD spectrum of the product collected from the T -swing test shown in (b), together with an XRD spectrum measured of the same solids after they have been put back into their liquor and maintained at the same high T and low CO₂ atmosphere for another 8 h. The first peak from the left shifted towards the right, i.e. towards the characteristic peak of hydromagnesite, indicating a slow transformation of dypingite to hydromagnesite over time.

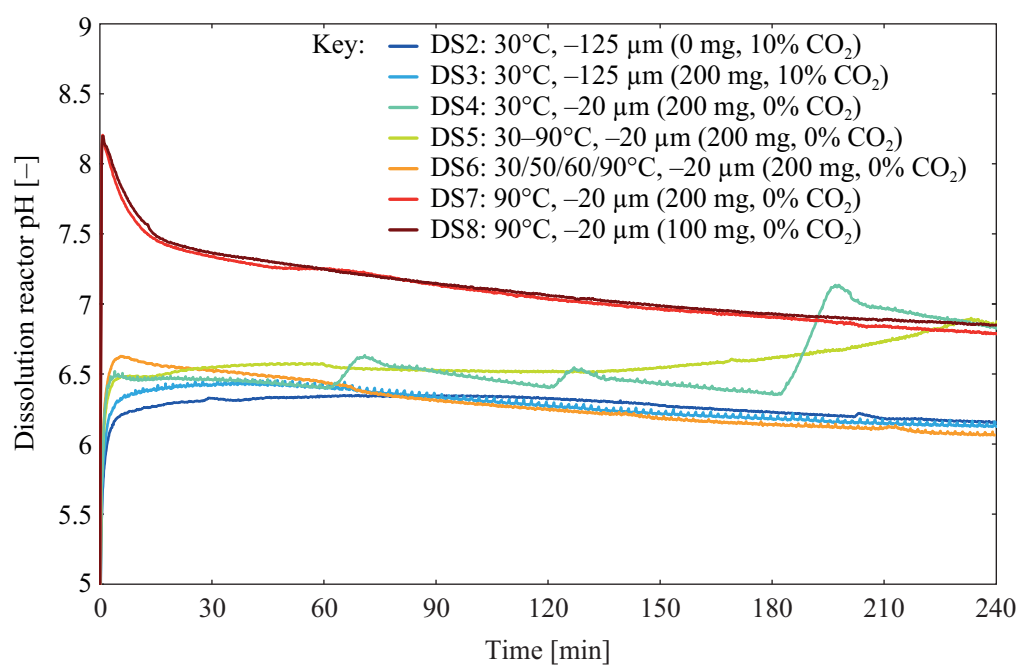


Fig. S2 The dissolution reactor pH over the entire runtime for all double-step experiments discussed in Section 5.2 with experimental conditions annotated in the key (precipitator conditions in parentheses)